Automotive Experiences
Vol. 9 No. 1 (2026) pp. 160-178
p-ISSN: 2615-6202 e-ISSN: 2615-6636

Research Paper

Crashworthiness and Failure Mechanism of Polylactic Acid Multi-Cell Tubes Hybridized with Aluminum/Copper Under Axial Compression

Muhammad Syaiful Fadly, **Khairil Anwar**, **Muhammad Sadat Hamzah**, **I Komang Diego Antara**

Department of Mechanical Engineering, Universitas Tadulako, Palu 94118, Indonesia

msfadly@untad.ac.id

https://doi.org/10.31603/ae.14485

Published by Automotive Laboratory of Universitas Muhammadiyah Magelang

Article Info
Submitted: 05/08/2025
Revised: 12/03/2026
Accepted: 30/03/2026
Online first: 31/03/2026

Abstract

This research investigates the crashworthiness performance and energy absorption behavior of crash boxes constructed from hybrid materials comprising Polylactic acid (PLA), aluminum (Al), and copper (Cu) under quasi-static axial compression. The crash box configuration comprises a PLA outer shell, an internal Al or Cu core, and PLA-based multi-cell structures with varying geometries, including circular, square, and hexagonal shapes. These components were fabricated through 3D printing and subjected to quasi-static axial compression testing. The experimental findings indicate that incorporating a hybrid core significantly enhances energy absorption capabilities. Among the tested configurations, the hexagonal multi-cell design exhibited the highest energy absorption, reaching 0.53 kJ. In addition, the CB-Al-H configuration, which uses an Al core, showed the highest specific energy absorption (SEA) of 77.77 kJ/kg and a crushing force efficiency (CFE) of 0.43%. This SEA value is approximately 69.17% higher than that of the copper-based configuration (CB-Cu-H), which recorded 45.98 kJ/kg with a CFE of 0.48%. The lower SEA observed in the copper-core configuration is primarily due to the higher Cu density, which increases the overall structural mass and consequently reduces specific energy absorption.

Keywords: Crashworthiness; Hybrid crash box; Polylactic acid; Quasi-static test; 3D printing; Energy absorption

1. Introduction

The rapid development of industrial technology has significantly expanded transportation systems, particularly in the automotive and high-speed rail sectors. While this progress improves mobility and efficiency, it also increases the risk of traffic accidents and safety concerns. To mitigate collision damage, energy-absorbing components are widely used to reduce impact forces and injury severity. Traditionally, these components are designed using simple thin-walled structures, such as circular or square tubes [1], [2], [3]. Integrating sacrificial thin-walled structures to absorb impact energy has become a common strategy to improve vehicle crashworthiness [4], [5]. However, single-cell tubes often exhibit inconsistent deformation patterns, leading to suboptimal energy absorption performance. In practical automotive crash box applications, engineers must balance several critical design constraints, including high energy absorption capability, controlled peak crushing force to reduce occupant deceleration, limited packaging space within bumper systems, and lightweight structural requirements. Conventional single-cell structures often struggle to simultaneously meet these engineering requirements, particularly in maintaining stable, progressive deformation while achieving high energy-absorption efficiency.

To enhance structural energy absorption, various innovative tube configurations have been developed, including multi-cell structures [6], [7], hybrid multi-cell designs [8], [9], bi-tubular systems [10], [11], conical geometries [12], [13], corrugated profiles [14], [15], [16], gradient wall thickness tubes [17], [18], and hierarchical structures [19], [20]. Several studies have explored hybrid structures combining circular tubes with multi-cell configurations. For example, Wu *et al.* [21] examined the influence of multi-cell topology on crashworthiness performance, while Chen *et al.* [22] analyzed hybrid multi-cell tubes combining circular and square geometries, focusing on crushing force and deformation behavior. Wirawan *et al.* [23] investigated circular aluminium–composite hybrid tubes reinforced with waru bark fiber layers, producing four configurations: aluminium circular tube (ACT), composite circular tube (CCT), hybrid inner circular tube (HICT), and hybrid outer circular tube (HOCT). Ardiansyah *et al.* [24] studied 3D-printed hybrid tubes made of PLA and PACF with shell thicknesses of 1, 1.5, and 2 mm under quasi-static axial loading. Zheng *et al.* [25] further investigated LVT multi-cell tubes and introduced hierarchical design principles to improve crashworthiness.

Recent studies focus on lightweight, eco-friendly materials such as PLA, which are compatible with fused deposition modeling 3D printing [26], [27], [28]. multi-cell crash boxes such as multi-cell circle, multi-cell square, multi-cell pentagonal, and multi-cell pentagonal circle were fabricated with 2 mm walls and 150 mm length [29], but low PLA strength requires enhancements. Hybrid cellular structures improve energy absorption and reduce density [30], [31], [32]. X. Fu *et al.* [31] reported a 28.4 percent improvement in force to displacement with thicker walls. Dony *et al.* [32] found that PLA - aluminium achieved the highest energy absorption of 428.01 J and crash force efficiency of 0.77, with only a 6.5 percent increase in peak force. Multi-cell structures are therefore considered an effective approach for improving energy absorption capacity and controlling failure mechanisms during axial impacts. Circular, square, and hexagonal multi-cell geometries provide different stress distributions, deformation behaviors, and structural stability. Previous studies have confirmed that internal crash box geometry strongly influences energy absorption efficiency and failure modes [33], [34], [35]. Combining these geometries with 3D-printed PLA and hybrid Al or Cu layers is expected to yield a lightweight, efficient crash box system. Therefore, this study investigates the crashworthiness performance and failure mechanisms of a hybrid multi-cell crash box made of 3D-printed PLA combined with Al and Cu under quasi-static axial loading. Three multi-cell geometries, circular, square, and hexagonal, are evaluated to identify the optimal design in terms of energy absorption efficiency, structural stability, and deformation behavior. The findings are expected to contribute to the development of lightweight and environmentally friendly structures for automotive, public transportation, and structural safety applications.

However, although hybrid PLA-metal structures and multi-cell configurations have been widely studied, most previous research has primarily focused on wall thickness variations, general hybrid designs, or material combinations. The influence of different multi-cell geometries within a hybrid PLA–metal crash box has not been systematically investigated. In particular, the interaction between multi-cell geometry and different metallic reinforcement layers in determining crashworthiness performance remains insufficiently understood. As a result, the role of multi-cell geometry in influencing energy absorption behavior and deformation mechanisms in hybrid PLA–metal structures is still limited. To address this gap, this study proposes a hybrid crash box structure fabricated from 3D-printed PLA, with Al and Cu layers, incorporating three internal multi-cell geometries: circular, square, and hexagonal. The novelty of this work lies in the systematic investigation of the combined effects of multi-cell geometry and hybrid metallic reinforcement on crashworthiness performance, including energy absorption capacity, deformation behavior, and failure mechanisms under quasi-static axial loading. The findings provide new insights into the design of lightweight hybrid crash box structures with improved energy-absorption performance.

2. Materials and Method

2.1. Materials

In this study, Al and Cu metal materials were used as the core or middle layer. Based on the results of material testing (**Figure 1**), the following material properties were obtained: density ϱ =

2,700 kg/m³, young's modulus E = 55.35 GPa, poisson's ratio ν = 0.33, yield stress σ_s = 300.25 MPa, ultimate stress σ_b = 415.78 MPa. Meanwhile, the properties of Cu material are as follows: density ϱ = 8,960 kg/m³, young's modulus E = 72.15 GPa, poisson's ratio ν = 0.33, yield stress σ_s = 420.64 MPa, ultimate stress σ_b = 530.22 MPa. The tensile tests for both Al and Cu were carried out according to ASTM E8/E8M using a Universal Testing Machine (UTM). The polylactic acid (PLA) filament utilized in this study has a diameter of 1.75 mm, and its mechanical properties were determined experimentally according to ASTM D638 using a UTM, as summarized in **Table 1**.

2.2. *Tube Geometry and Design Parameters*

This study introduces a hybrid material concept that integrates a multi-cell structural design. The proposed configuration features an Al/Cu-based shell combined with a multi-cell core, utilizing three distinct internal geometries (**Figure 2**). Each shape serves a unique mechanical purpose, the circular design promotes uniform stress distribution, the square enhances localized stiffness. At the same time, the hexagonal structure offers improved energy absorption by accommodating deformation along multiple directions. The sample configuration is shown in **Figure 3**.

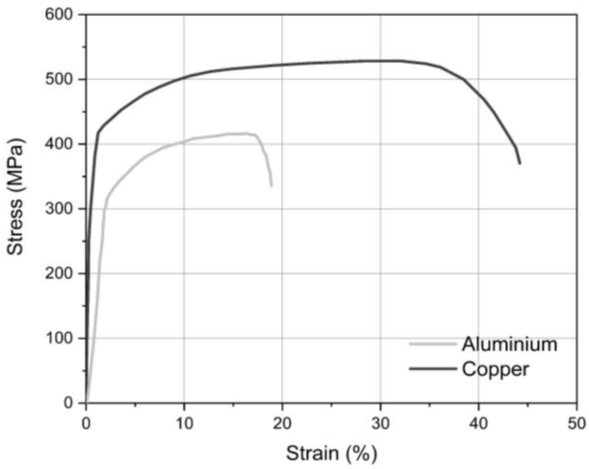

Figure 1. Stress–strain response of Al and Cu materials

Table 1. Material properties of the PLA specimen

Density (g/cm³)	Tensile strength (MPa)	Elongation (%)	Flexural strength (MPa)	Flexural modulus (MPa)
1.24	24.12	6.21	104.33	2875.21

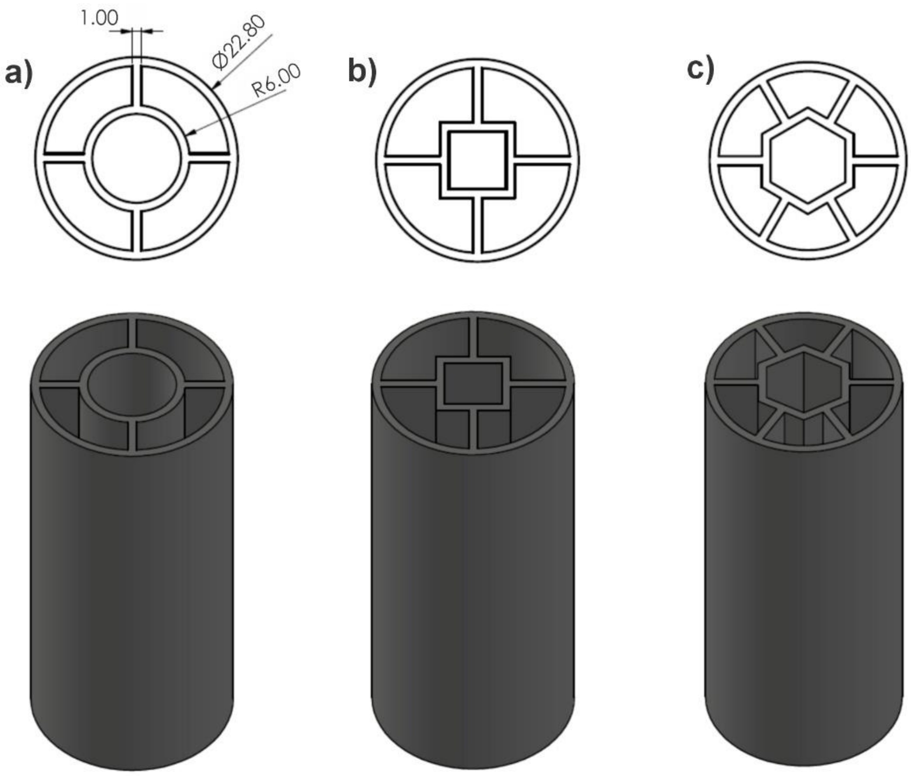

Figure 2. Multi-cell geometric designs (unit: mm): (a) Circular; (b) Square; (c) Hexagonal

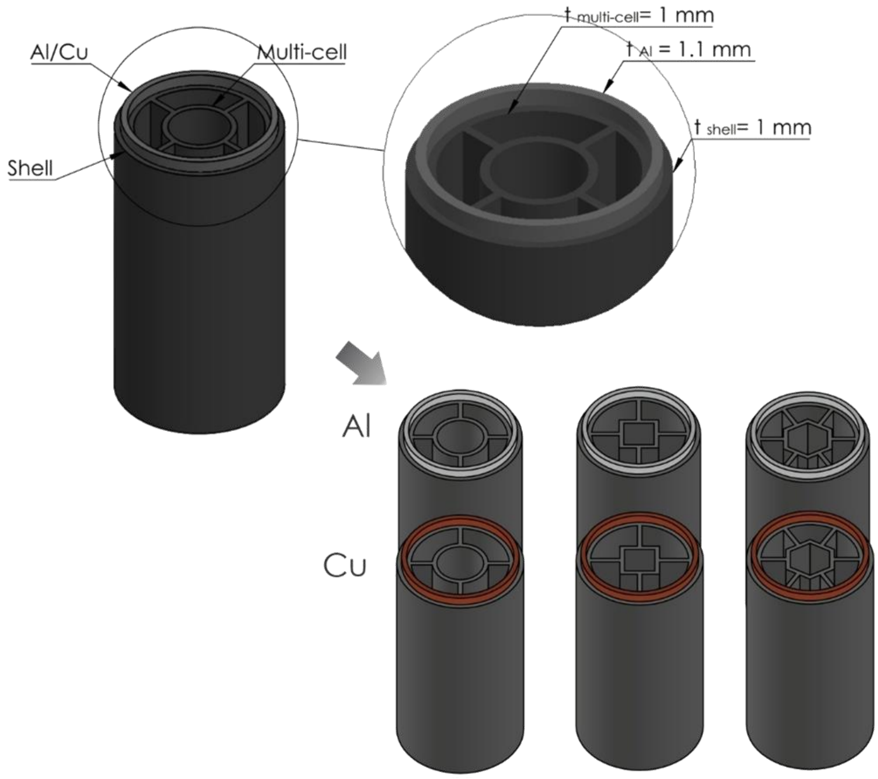

Figure 3. Hybrid tube specimens

In this study, Al and Cu tubes with a diameter of 1.1 mm were utilized as the outer layer in the hybrid structural configuration. Both the shell and multi-cell components were designed with a length of 50 mm, while the Al and Cu tubes were fabricated 2 mm longer to function as initial crushing triggers. This slight length difference allowed the metallic tubes to initiate deformation earlier during axial loading. According to previous studies [36] the global peak crushing force (GPCF) is typically observed in multi-cell specimens either when equipped with an initiator at the ends or when designed with tapered terminations.

The multi-cell cores were fabricated with an external diameter of 22.8 mm and a wall thickness of 1 mm, ensuring a press-fit engagement with the inner diameter of the Al and Cu tubes. This tight interference fit was achieved manually by applying uniform compression during assembly. Similarly, the PLA-based shell structures were produced with an internal diameter of 24.9 mm and a 1 mm wall thickness to establish a snug fit within the outer metallic tubes. The assembly of both the multi-cell core and outer shell structures was performed using a manual press-fitting method. The metallic cores were inserted into the PLA structures with a controlled interference fit, with an approximate dimensional tolerance of about 0.1-0.2 mm between the components to ensure sufficient contact at the interface. The insertion was carried out using a manual pressing process to achieve a tight mechanical fit without the use of adhesives, thereby maintaining consistent interface conditions among all specimens. A total of twelve distinct hybrid specimen configurations were prepared for testing, as detailed in **Table 2**.

2.3. *Manufacturing Process for Crashworthiness Specimens*

The shell and multi-cell components were fabricated using the fused deposition modeling (FDM) technique, employing a Bambu Lab 3D printer, as illustrated in **Figure 4**.

In this process, PLA filament is heated to its melting temperature within the extruder nozzle and then deposited layer by layer onto the build platform. The printer uses motion along the XY axes to define the geometry of each layer. In contrast, vertical motion along the Z-axis enables layer accumulation to achieve the desired structural height of 50 mm. The specimens were fabricated using a raster angle of ±45° with three outer perimeters to enhance structural stability. A layer height of 0.2 mm and 100% infill density were applied to ensure consistent mechanical performance. The printing temperature was set to 220 °C, with a bed temperature of 60 °C, to promote adequate inter-layer bonding and reduce the risk of delamination during axial compression. The detailed printing parameters used to produce the crashworthiness specimens are presented in **Table 3**. **Figure 5** presents the quasi-static test specimens used to evaluate the crashworthiness performance in this study.

2.4. Axial Compression Testing under Quasi-Static Conditions

Quasi-static axial compression tests were carried out in this work using a universal testing machine (UTM). Each specimen was placed on a stationary base, and the compression was applied using a rigid indenter that moved downward at a controlled rate of 2 mm/s, as shown in **Figure 6**. For each configuration, three specimens were tested (n = 3) in order to obtain the average values of the measured parameters and improve the reliability of the experimental results. The quasi-static loading rate of 2 mm/s was selected based on common practice in crashworthiness testing of thin-walled structures and 3D-printed polymer components reported in previous studies [23]. Throughout the testing process, sequential photographs were captured to monitor the progression of deformation and to assess the specimen's fracture behavior and resistance to compressive loading.

Table 2. Crashworthiness sample configurations

Specimen Crashworthiness	Code	Diameter (mm)	Thickness (mm)	Mass (g)
Aluminium-Tube	Al-T	25.1	1.1	19.1
Copper-Tube	Cu-T	25.0	1.1	42.9
PLA-Tube	PLA-T	27.2	1.0	7.2
Multi-Cell Circular	MCC	22.8	1.0	12.4
Multi-Cell Hexagonal	MCH	22.8	1.0	13.2
Multi-Cell Square	MCS	22.8	1.0	12.7
Crash Box-Aluminium-Circular	CB-Al-C	27.1	3.1	36.4
Crash Box-Aluminium-Hexagonal	CB-Al-H	27.0	3.1	37.6
Crash Box-Aluminium-Square	CB-Al-S	27.0	3.1	36.3
Crash Box-Copper-Circular	CB-Cu-C	27.0	3.1	52.1
Crash Box-Copper-Hexagonal	CB-Cu-H	27.1	3.1	53.4
Crash Box-Copper-Square	CB-Cu-S	27.0	3.1	52.2

Figure 4. Fabrication process using 3D Printing: (a) Bambu lab software; (b) Printing process; (c) Multi-cell tube; (d) shell tube

Table 3. 3D Printing parameters for shell and multi-cell fabrication

Parameter	Setting
Nozzle temperature	220 °C
Filament width	0.2 mm
Layer height	0.2 mm
Fill density	100%
Printing speed	185 mm/s
Layer orientation	X-axis
Infill pattern	Rectilinear
Slice	Ultra-High Quality
Support material	PLA filament
Build plate temperature	60 °C

Figure 5. Crashworthiness specimens: (a) Al-T; (b) CB-Al-C; (c) CB-Al-S; (d) CB-Al-H; (e) Cu-T; (f) CB-Cu-C; (g) CB-Cu-S; (h) CB-Cu-H

2.5. *Crashworthiness Performance*

Several key indicators are commonly employed to assess a structure's resistance to impact, including specific energy absorption (SEA), mean force (MF), initial peak force (IPF), crushing force efficiency (CFE), and overall energy absorption (EA) [37], [38], [39]. Among these, EA represents the total amount of energy dissipated during the deformation process, typically quantified by the area enclosed beneath the load-displacement curve. This energy metric can be mathematically described through the following integral expression, shown in Eq. (1).

$$EA = \int_0^{\delta_1} P\,(\delta)\,d\delta \qquad (1)$$

where EA is the energy absorption (J), P is the applied load (N), and δ is the displacement (m). Once the total energy absorption (EA) is determined, the specific energy absorption (SEA) can subsequently be calculated. SEA refers to the amount of energy absorbed per unit mass of the specimen, serving as a key metric for evaluating energy efficiency relative to weight. It is mathematically defined as follows Eq. (2).

$$SEA = \frac{\int_0^{\delta} P\,(\delta) d\delta}{m} = \frac{EA}{m} \qquad (2)$$

where SEA is the specific energy absorption (J/kg), EA is the total energy absorbed (J), m is the mass of the specimen (kg). The Mean Force (MF) refers to the average load sustained by the structure during the deformation process as the energy absorber approaches a stable crushing state. This parameter can be quantitatively expressed using the following Eq. (3).

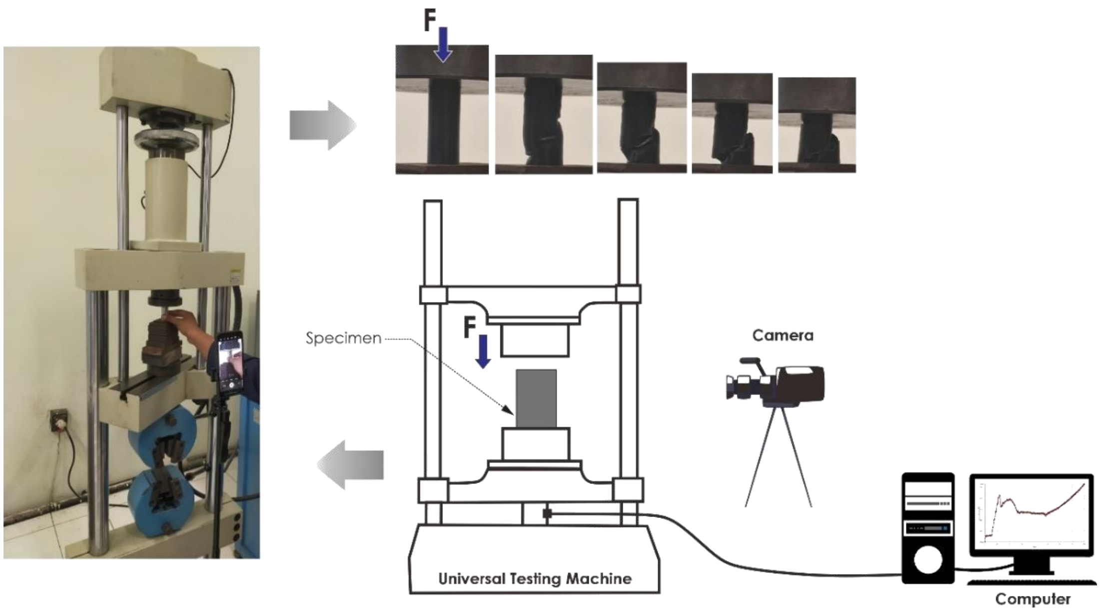

Figure 6. Quasi-static testing method for crashworthiness evaluation

$$MF = \frac{\int_0^{\delta} P\,(\delta) d\delta}{\delta max} = \frac{EA}{\delta_{max}} \quad (3)$$

where EA is the total energy absorbed (J) and δmax denotes the maximum displacement (m). Crushing force efficiency (CFE) is a dimensionless parameter that reflects the uniformity of force distribution during deformation. It is calculated as the ratio between the mean crushing force (MF) and the initial peak force (IPF), providing insight into the stability and effectiveness of the energy absorption process, as presented in Eq. (4).

$$CFE = \frac{MF}{IPF} \times 100 \quad (4)$$

3. Results and Discussion

3.1. Crashworthiness of Aluminum and Copper Tubes

Quasi-static testing plays a crucial role in evaluating the potential impact of strain rate on both the Al core and the Cu tube, as previously reported in related studies [39], [40]. The outcomes of these tests, including the load–displacement responses and corresponding deformation patterns, are presented in **Figure 7**.

Figure 7 presents the load-displacement curves obtained from the quasi-static compression tests. At the onset of loading, a considerable amount of force is needed to initiate deformation in the tube, resulting in a pronounced initial peak force. This stage marks the commencement of the energy absorption process, during which the impactor initiates progressive plastic deformation. As the folding mechanism develops, each successive deformation stage contributes to variations in the reaction force, which is reflected as a fluctuating load response across the displacement. This pattern is consistently observed across all crashworthiness configurations, indicating the typical behavior of thin-walled structures under axial loading conditions.

As shown in **Figure 7a**, the Al tube exhibits a distinct load-displacement profile characterized by a sharp initial peak, which signifies the maximum load the structure can withstand before undergoing plastic deformation. This peak typically marks the onset of structural instability, after which the load response enters a fluctuating pattern, reflecting successive folding events as the tube progressively collapses. Following the initial load drop, a secondary plateau emerges, indicating the formation of the first fold and the beginning of a more stable deformation regime. With continued displacement, multiple folding stages develop in sequence, eventually producing a regular axisymmetric concertina pattern. Such a deformation mode aligns with classical observations of thin-walled tube behavior under quasi-static compression, where energy absorption occurs through repeated cycles of folding and localized buckling [40], [41].

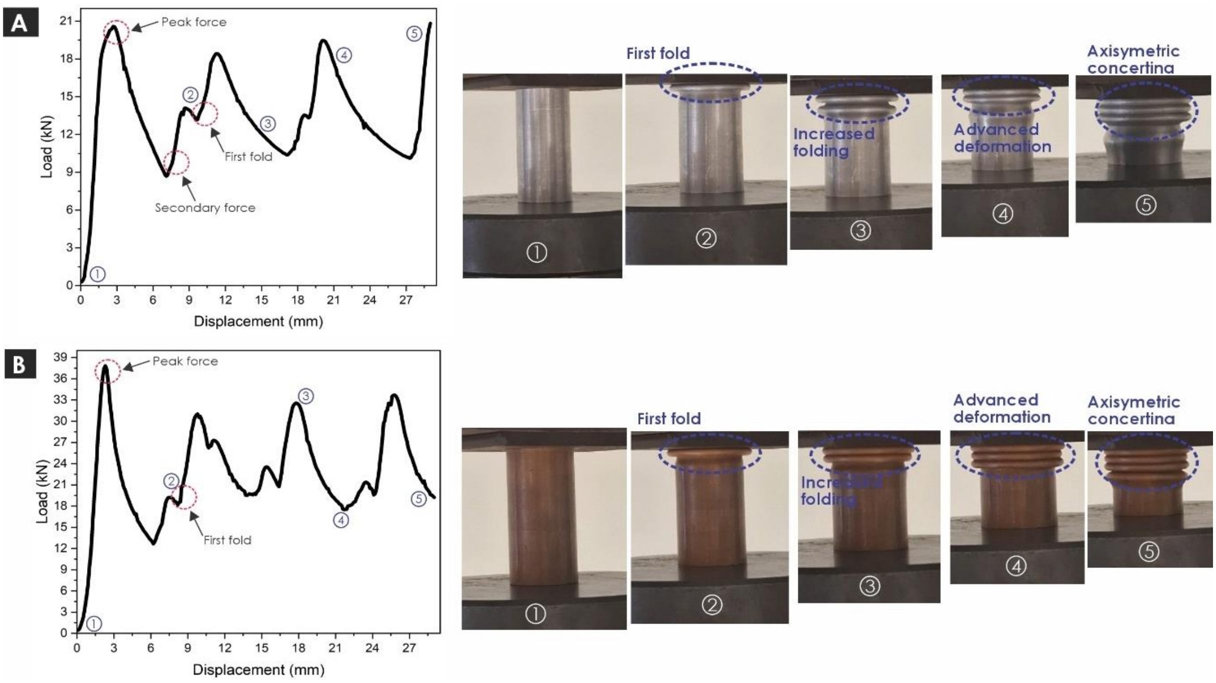

Figure 7. Quasi-static load: (a) Al-T; (b) Cu-T

In comparison, the Cu tube shown in **Figure 7b** demonstrates a significantly higher initial peak force, which can be attributed to its enhanced yield strength and notable strain hardening behavior. While the general folding sequence mirrors that observed in the Al specimen, the Cu tube displays greater load oscillations throughout the deformation process. These pronounced fluctuations suggest a more substantial capacity for energy absorption and release, indicative of a robust deformation mechanism. Additionally, the Cu tube exhibits a more consistent and symmetrical concertina folding pattern, which highlights its structural stability under compressive loading. The ability to sustain higher mean force levels with minimal irregularities throughout the collapse process reflects superior crashworthiness characteristics. These observations are in agreement with those of Liu *et al*. [42] who noted that the ductility and strain rate sensitivity of a material play critical roles in determining both the folding mode and the efficiency of energy dissipation during axial compression.

3.2. *Crashworthiness of Multi-cell Tubes*

Figure 8 illustrates the load-displacement response of the 3D-printed multi-cell structure, fabricated using PLA material, with three distinct geometric configurations: MCC, MCS, and MCH. As illustrated in **Figure 8**, the MCS configuration exhibits the most stable displacement profile following the initial peak, indicating a consistent and progressive folding mechanism, as well-distributed internal stresses during compression. In contrast, the MCC and MCH specimens display a more pronounced load drop accompanied by substantial fluctuations, indicating localized damage and structural instability throughout the crushing process. This observation aligns with the findings of Chen and Wierzbicki who emphasized that symmetric internal partition walls in multi-cell configurations can significantly enhance energy absorption performance by preventing early-stage cracking and asymmetric deformation [43]. Within this context, the MCS design maintains its structural rigidity more effectively compared to MCC and MCH, both of which suffer from performance degradation due to uncontrolled deformation following peak load. The MCS specimen exhibits a peak reaction force of 4.54 kN, with the first sign of folding observed at a displacement of 9.2 mm.

In the MCC design, local buckling becomes evident under compressive loading, initiating a fold around 7 mm of displacement. Meanwhile, the MCH configuration achieves the highest peak load of 5.06 kN. The deformation in this case begins with localized buckling at 10.1 mm and progresses steadily until total wall collapse occurs at 29 mm. Despite all designs demonstrating the ability to absorb impact energy, the peak force responses across configurations are inconsistent and irregular. This variation is likely attributed to the inherent progressive failure behavior of the PLA material, which tends to deform nonlinearly under load, as also noted by Li *et al*. [44]. A portion of the impact energy is dissipated during the onset of local deformation before the structure reaches its final collapse state.

Figure 9 provides visual confirmation of the deformation sequences corresponding to the quantitative trends observed earlier. The MCC configuration exhibits early failure initiated by local buckling, which progresses into asymmetric folding and shear-induced cracking, ultimately leading to a complete fracture of the outer shell. In contrast, the MCS specimen exhibits a more controlled and stable collapse behavior, characterized by symmetric folding patterns throughout the compression process. Although some wall flattening becomes apparent at the final stage, likely due to accumulated plastic strain, no significant structural damage is visible prior to that. The MCH variant, however, undergoes initial

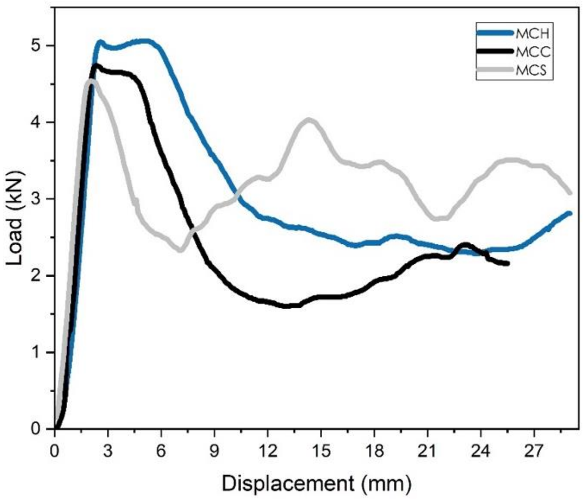

Figure 8. Load-displacement behavior of multi-cell 3d-printed PLA structures

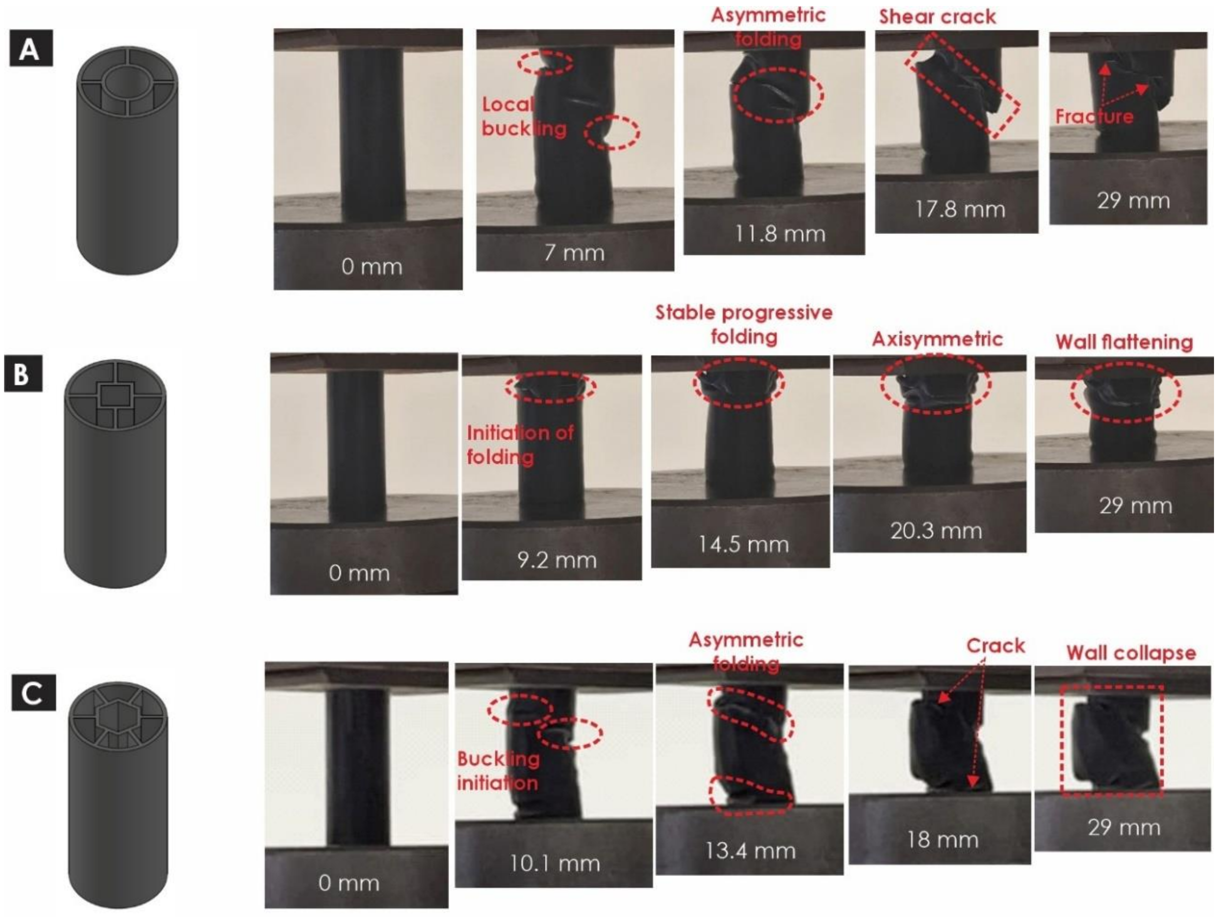

Figure 9. Quasi-static load: (a) MCC; (b) MCS; (c) MCH

instability marked by uneven buckling and non-uniform folding. This evolves into visible cracking and culminates in complete wall collapse, primarily due to concentrated stress in localized regions. These observations reinforce the critical role of geometric configuration in dictating how deformation propagates during crushing. Such behavior aligns with findings from Tripathi *et al*. [45] who reported that in geometrically complex structures, such as honeycomb-based systems, the absence of internal symmetry often results in inconsistent stress pathways, thereby compromising structural integrity under load.

3.3. *Crashworthiness of Hybrid Tubes*

Figure 10 illustrates the load-displacement response of the hybrid crash box structure, which features a combination of a PLA shell, a metal core (Al or Cu), and a PLA multi-cell configuration inside. In the Al-based system (**Figure 10a**), the hexagonal multi-cell configuration (CB-AL-H) recorded the highest first peak force of 23.85 kN at a displacement of 4.9 mm, followed by the circle configuration (CB-AL-C) with a first peak of 22.56 kN, and finally the square configuration (CB-AL-S) of 19.39 kN. In the Cu-based system (**Figure 10b**), the peak force values increased significantly. CB-CU-S recorded a first peak of 35.51 kN, followed by CB-CU-C at 34.51 kN, and CB-CU-H at 32.98 kN. The difference in initial peak force between hybrid structures and single-core specimens is due to interactions between failure mechanisms in the materials. In single-core specimens, the axial load is applied directly to the metal, allowing stiff materials such as Cu to reach their maximum resistance almost instantly. In hybrid configurations, the load is distributed across the interface between the multi-cell PLA shell and the metal core. Surface irregularities can lead to non-simultaneous loading, causing the PLA shell to experience local failure or micro-buckling before the metal core reaches its peak force, slightly reducing the overall peak force, as observed in CB-Cu-S. **Figure 11** illustrates the deformation stages and types of failure that occur during the quasi-static compression process.

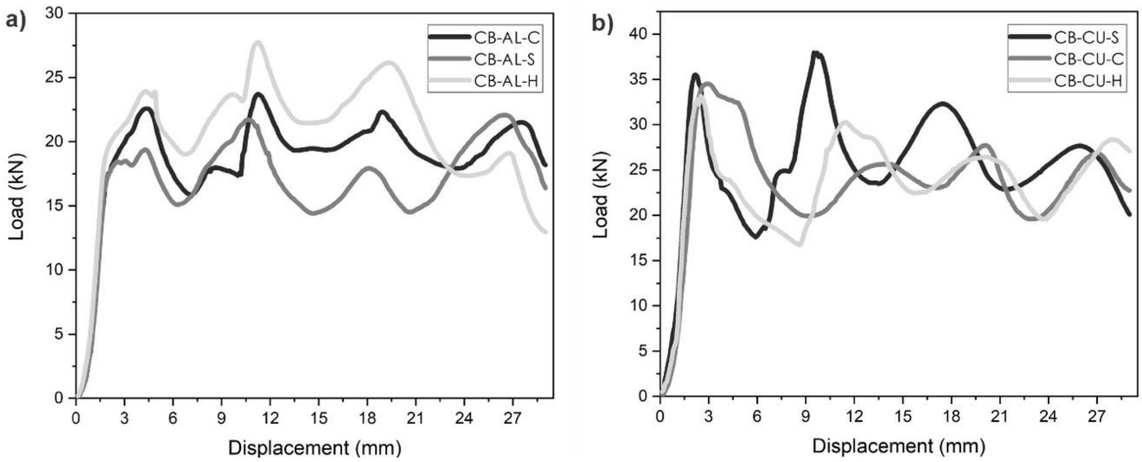

Figure 10. Load-displacement response of hybrid tube: (a) Al core; (b) Cu core

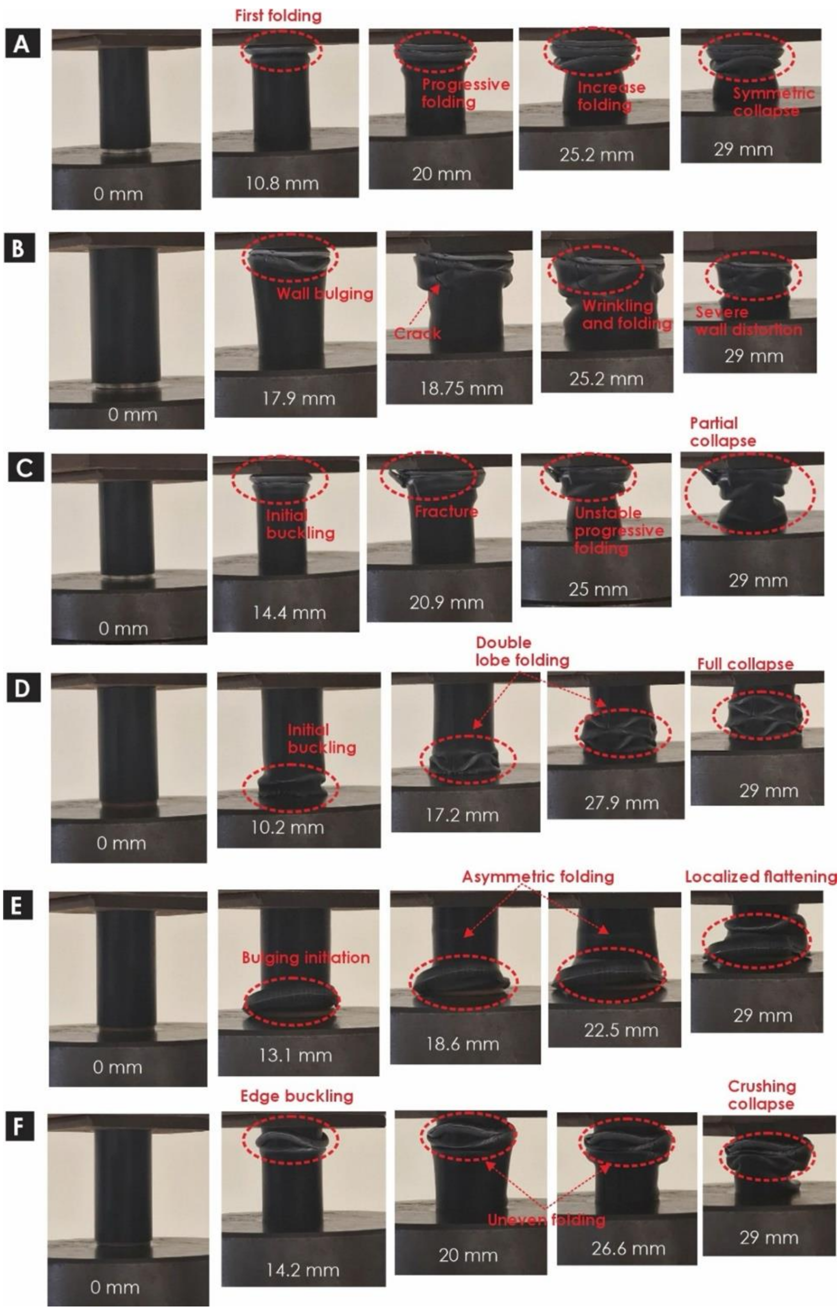

Figure 11. Quasi-static load: (a) CB-Al-C; (b) CB-Al-S; (c) CB-Al-H; (d) CB-Cu-C; (e) CB-Cu-S; (f) CB-Cu-H

The CB-AL-C configuration exhibited symmetrical and progressive folding, which began at 10.8 mm and continued steadily until reaching 29 mm, indicating stable performance despite having a lower peak force. CB-AL-S experienced wall bulging, cracking, and severe distortion at displacements of 17.9-29 mm, indicating stress concentration at the corners of the square geometry that triggered local failure. In the hexagonal configuration (CB-AL-H), deformation began at 14.4 mm, followed by fracture and unstable folding, resulting in partial collapse. This condition indicates that although the hexagonal configuration can withstand high initial loads, the irregularity of the stress distribution renders it susceptible to asymmetric failure. Liang *et al*. [46] stated that internal structures with angular geometry tend to experience stress concentration at the edges, which can cause uncontrolled deformation if not supported by internal symmetry and an optimal cross-section design.

The Cu-based configurations exhibited more complex failures due to the high stiffness of the metal core. CB-CU-C exhibited initial buckling at 10.2 mm and double lobe folding, which ended in complete collapse at 29 mm. CB-CU-S experienced bulging, asymmetric folding, and localized flattening since 13.1 mm, indicating the uneven deformation due to the square corners that accelerated the local failure. Meanwhile, the CB-CU-H configuration experienced edge buckling and uneven folding, followed by crushing collapse, starting at a displacement of 14.2 mm.

3.4. Crashworthiness Characteristics

The performance characterisation of hybrid tube structures with circular, square, and hexagonal shell-Al/Cu-multi-cell configurations is presented comprehensively in **Figure 12**. This evaluation encompasses key parameters, including energy absorption capacity (EA), mean force (MF), specific energy absorption (SEA), and crushing force efficiency (CFE). This analysis provides an in-depth overview of structural efficiency and energy absorption capabilities, which play a crucial role in determining the effectiveness and reliability of hybrid tube designs under specific loading conditions.

Figure 12a shows that the CB-Cu-H design exhibited the highest energy absorption capacity, with an average value of 1.86 kJ. In contrast, the lowest energy absorption was observed in the CB-Al-C configuration, with an average value of 1.50 kJ. The measured values across the tested specimens showed standard deviations ranging from ±0.15 to ±0.47 kJ. The enhanced performance of the CB-Cu-H model can be attributed to the presence of a Cu layer at the midsection, coupled with a hexagonal multi-cell structure on the interior, which provides improved load distribution and structural integrity during axial compression. From a mechanical perspective, the higher EA observed in the CB-Cu-H configuration is related to a more uniform stress distribution within the multi-cell network during progressive collapse. The hexagonal geometry allows the compressive stresses to be transferred along multiple inclined cell walls, reducing localized stress concentrations and promoting stable progressive folding. As a result, plastic deformation develops gradually along the tube length, enabling continuous energy dissipation throughout the crushing process. The ability of a structure to absorb energy is closely linked to the magnitude of the applied load. Higher loads generally lead to an increase in energy dissipation, mainly when supported by optimised internal geometries and material combinations.

Additionally, the inclusion of reinforcing layers within the crash box plays a crucial role in enhancing its resistance to impact forces, as documented in prior studies [47], [48]. Another contributing factor is the interaction between the ductile Cu core and the surrounding PLA multi-cell shell. Cu has higher ductility and plastic deformation capacity than Al, allowing the metal core to sustain large plastic strains while the PLA cell walls stabilize the folding pattern. This interaction delays catastrophic buckling and supports progressive deformation, which directly increases the absorbed energy. In the CB-Cu-H configuration, the increase in energy absorption can also be associated with the expansion of the deformed cross-sectional area within the internal tube wall during compression. This expansion contributes to an increase in the moment of inertia, thereby enhancing the structure’s resistance to buckling and progressive collapse. As stated in Euler’s theory, the critical load that a structure can withstand is directly proportional to its moment of inertia; thus, a higher moment of inertia results

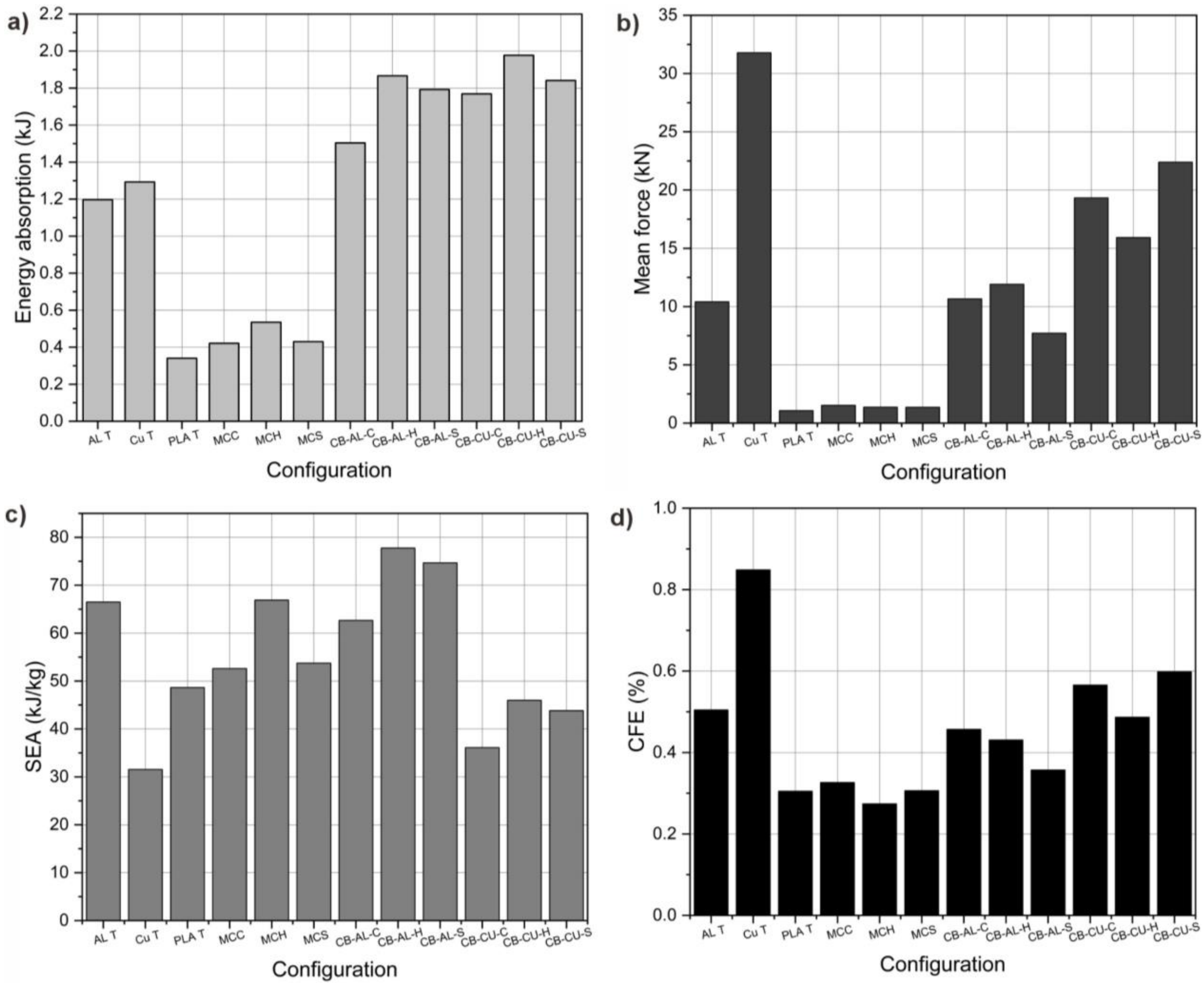

Figure 12. (a) Energy absorption; (b) Mean force; (c) Specific energy absorption; (d) Crush force efficiency

in an improved load-bearing capacity and, consequently, higher energy absorption. Furthermore, the presence of multiple internal cell walls increases the number of plastic hinge formation sites during collapse. These hinges form at the intersection of cell walls and geometric corners, which serve as controlled stress-concentration points. Instead of causing premature fracture, these locations guide the folding pattern and contribute to a stable, progressive crushing mechanism, thereby enhancing the overall EA performance.

These results reinforce the effectiveness of combining ductile materials, such as Cu, with structurally stable geometries, like hexagonal cells, for crashworthiness applications. From an automotive design perspective, crash box structures are expected to absorb impact energy efficiently while maintaining peak force levels within acceptable limits to minimize excessive deceleration transmitted to the vehicle occupants. In addition, practical design considerations such as packaging space within the front or rear bumper system and the need to achieve lightweight structural components are critical factors in crash box development. The hybrid PLA–metal multi-cell structure proposed in this study demonstrates potential advantages in meeting these requirements due to its relatively lightweight configuration and its ability to provide controlled progressive deformation under axial loading. Therefore, the integration of optimized multi-cell geometry with hybrid material reinforcement may contribute to the development of efficient energy-absorbing structures that support both structural safety and weight reduction in automotive applications. Not only does this combination improve overall impact energy dissipation, but it also enhances the deformation behaviour and load resistance characteristics of the hybrid tube.

The mean force values for each crash box configuration were determined based on the load-displacement curves, calculated as the average force amplitude throughout the progressive folding process. This region represents the oscillating force required to initiate and sustain plastic deformation, effectively reflecting the structure's ability to resist axial collapse. A strong correlation was observed between MF and EA, with higher average forces generally corresponding to greater energy dissipation. Among the evaluated configurations, the CB-Cu-S design exhibited the highest mean force at 22.40 kN, while the CB-Al-S variant demonstrated the lowest value at 7.72 kN.

The results presented in **Figure 12c** and **Figure 12d** reveal key performance indicators related to energy absorption and crushing behaviour, namely SEA and CFE. Among the tested configurations, the hybrid structure CB-AL-H demonstrates the highest SEA value at 77.77 kJ/kg, indicating superior energy absorption per unit mass. Interestingly, a slightly higher SEA is observed in CB-CU-H at 79.6 kJ/kg, suggesting that while Al-honeycomb hybrids offer an optimal balance between mass and performance, Cu-based hybrids can also yield high absorption values despite their relatively greater density. The CB-AL-S configuration follows closely, with an SEA of 74.67 kJ/kg, confirming the effectiveness of square multi-cell designs in efficiently dispersing impact loads.

In evaluating the crushing stability and consistency of these hybrid structures, CFE becomes a critical parameter. This metric, derived from the ratio of the mean crushing load to the initial peak load, provides insight into how effectively a structure maintains force levels throughout the deformation process. A higher CFE indicates more stable and progressive folding, which is desirable in crashworthy components. Among the tested specimens, CB-CU-S records the highest CFE at 0.59%, highlighting its efficient load transfer and controlled collapse behaviour. On the other end of the spectrum, CB-Al-S exhibits the lowest CFE of 0.35%, indicating that the circular cell geometry, combined with a denser Cu shell, may lead to greater force fluctuations and less efficient energy distribution during crushing. In configurations with lower CFE, unstable folding behaviour can occur due to uneven stress distribution and localized buckling of thin PLA cell walls. When the internal geometry cannot effectively guide the progressive folding mechanism, the crushing force fluctuates significantly, reducing its efficiency despite acceptable energy absorption levels.

3.5. Deformation Characteristics under Crash Loading

Figure 13 shows the cross-sectional placement patterns of the feasibility structures with aluminium (Al-T) and copper (Cu-T) metal cores after being subjected to quasi-static loading. The second structure exhibits a typical concertina folding pattern, indicative of a controlled plastic solidification mechanism in the thin-walled tubular structure.

Figure 14 shows that the circular configuration exhibits symmetric and progressive deformation, indicating an efficient and gradual energy absorption mechanism. However, there are indications of delamination between the PLA and Al due to stress concentration during intense folding. This behaviour is likely associated with the modulus mismatch between PLA and Al, which can generate interfacial shear stresses during the progressive folding process and weaken the adhesion at the interface. Meanwhile, the square shape experiences asymmetric deformation (asymmetric folding) and local collapse at the corners of the internal structure, causing PLA fragmentation and premature destruction, indicating high energy absorption but structural instability. The localized crushing observed in this configuration also increases shear stress concentration at the PLA–metal interface, which may further promote interfacial separation.

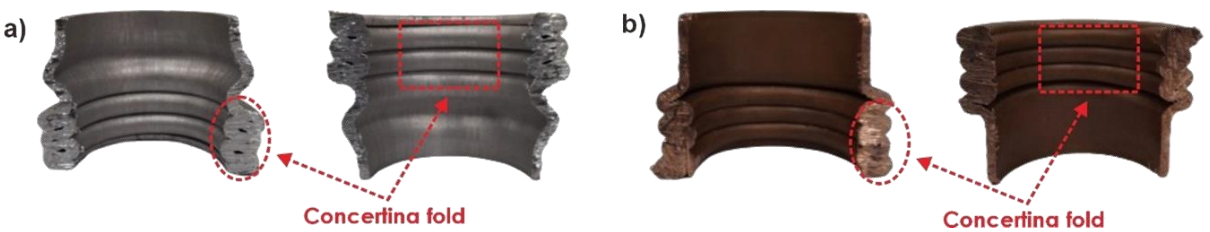

Figure 13. Crashworthiness deformation cross-section: (a) Al-T; (b) Cu-T

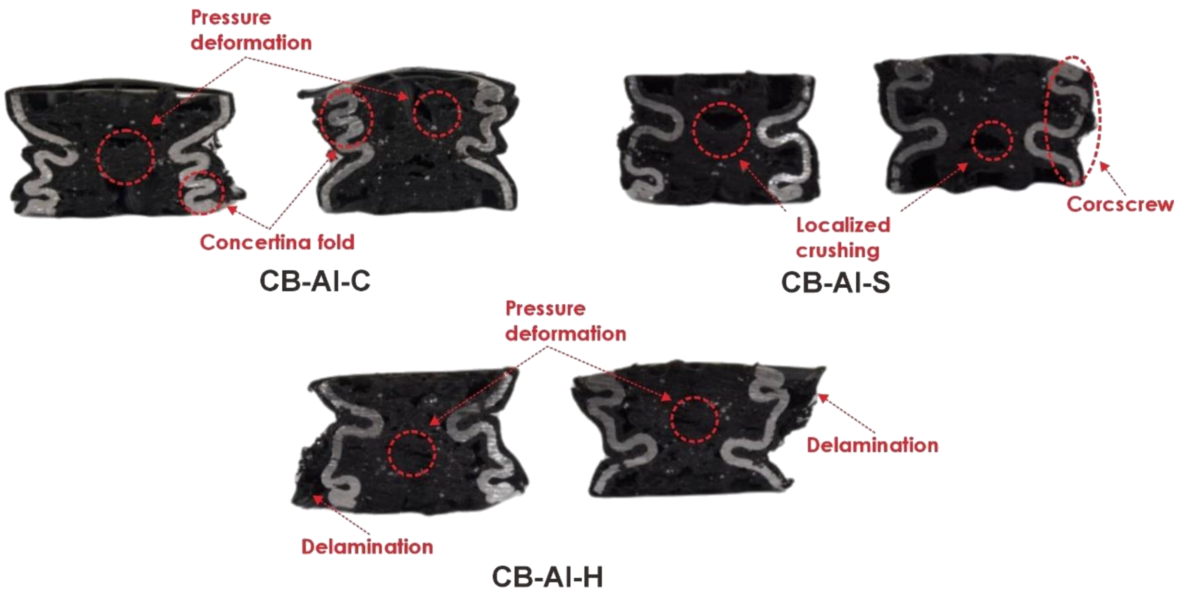

Figure 14. Crashworthiness deformation cross-section of the aluminum-core structure

In contrast to the previous two configurations, the hexagonal structure exhibits uniform and controlled progressive folding behaviour, characterised by a relatively even distribution of folds without significant damage to the outer wall, which reflects the efficiency of the hexagonal geometry in distributing stress optimally. Although this configuration demonstrates more stable deformation behaviour, minor delamination is still observed in several regions, suggesting that the interfacial bonding strength between PLA and Al remains a critical factor influencing the crashworthiness response. To further improve the structural performance, potential design strategies such as surface roughening of the metallic layer, the use of adhesive interlayers, or the incorporation of mechanical interlocking features could be considered to enhance interfacial adhesion and reduce the likelihood of delamination during axial compression.

Figure 15 shows that the failure behaviour is significantly influenced by the geometry of the multi-cell (circular, square, and hexagonal). In the circular configuration, symmetrical progressive folding occurs with a relatively stable radial deformation pattern; however, indications of delamination between the PLA and Cu layers suggest adhesion failure due to shear stress during the folding process. For the square structure, asymmetric damage, cracks in the inner walls, and uncontrolled compression are observed, leading to premature failure at the corners of the cells. Meanwhile, the hexagonal configuration shows a more even and gradual folding distribution. Still, it shows non-uniform failure on the outer side, likely due to stress accumulation at the junction points of the corners. This finding is consistent with the study by Heimbs *et al*. [49] which states that core materials with low elastic modulus tend to increase local deformation and reduce folding controllability, particularly when not supported by a symmetrical internal structure.

Figure 16 presents the CFE–SEA performance curves for the various hybrid tube configurations tested in this study. Based on the results, the CB-Al-H configuration demonstrates the best overall performance, achieving the highest specific energy absorption (SEA) of 77.77 kJ/kg with a CFE value of 0.43%. Although the CB-Al-S configuration shows a competitive SEA of 74.67 kJ/kg, its lower CFE value (0.35%) indicates less stable load distribution compared with the other Al-based variants. On the other hand, the CB-Cu-C configuration exhibits the lowest specific performance, with an SEA value of 36.10 kJ/kg. This is mainly attributed to the significantly higher density of Cu compared with Al, which reduces mass-based energy absorption efficiency (SEA), even though Cu-based configurations generally show higher CFE values (above 0.48%), indicating more consistent crushing force stability. The data distribution also suggests that hexagonal geometries (CB-Al-H and CB-Cu-H) tend to produce a more balanced performance

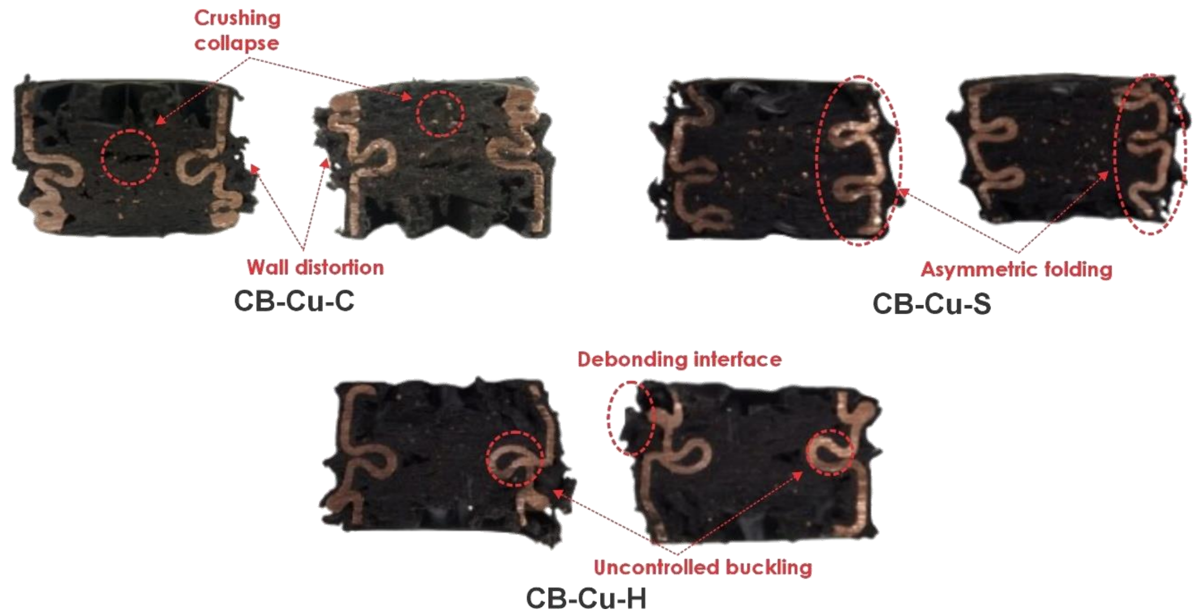

Figure 15. Crashworthiness deformation cross-section of the copper-core structure

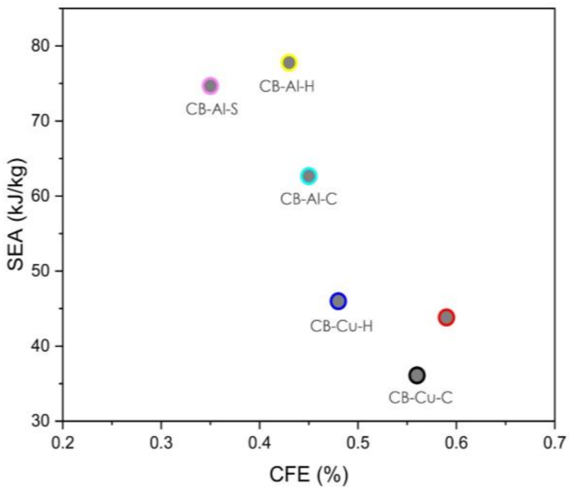

Figure 16. CFE–SEA performance curve

profile than the other geometries. These results highlight that an increase in crushing force efficiency (CFE) does not always correspond to an improvement in specific energy absorption (SEA). Instead, the selection of a low-density core material remains a dominant factor in achieving higher SEA values. Several studies have demonstrated that while increasing the wall thickness of Al tubes enhances their energy absorption capacity and load resistance, it often leads to a reduction in CFE, primarily due to the accompanying rise in the initial peak force during compression [50], [51].

4. Conclusion

The experimental results demonstrate that hybrid PLA–metal multi-cell crash boxes significantly improve crashworthiness performance compared with single-material configurations. Among the tested specimens, the CB-Cu-H configuration shows the highest energy absorption (EA = 1.97 kJ), indicating its superior ability to dissipate impact energy through stable progressive deformation. Although CB-Cu-H provides the highest EA, its peak force (Fmax = 33.18 kN) is still relatively high compared with that of Al-based hybrid structures. In contrast, the CB-Al-H configuration exhibits a more balanced performance, with high energy absorption (EA = 1.86 kJ), the highest specific energy absorption (SEA = 77.77 kJ/kg), and a lower peak force (F_{max} = 27.73 kN). This lower peak force is advantageous because it helps reduce the transmitted impact load while still maintaining effective energy dissipation. Therefore, although the CB-Cu-H configuration provides the maximum energy absorption capacity, the CB-Al-H configuration can be considered a more optimal crashworthiness design because it offers a better balance between energy absorption efficiency and a lower peak force response.

Despite these promising results, several limitations should be acknowledged. First, the present study was conducted only under quasi-static loading conditions, which may not fully represent the dynamic behaviour experienced during real crash events. Second, the mechanical response of PLA is sensitive to factors such as strain rate, temperature, and manufacturing-induced anisotropy, which may influence the overall crashworthiness performance. In addition, the experiments were performed on relatively small-scale specimens, which may not completely reflect the behaviour of full-scale automotive crash box components. Therefore, future research should focus on dynamic impact testing to better simulate real crash conditions, improving the interfacial bonding between PLA and the metallic layer to reduce delamination, and conducting numerical or finite element (FE) simulations to validate and extend the experimental findings. Such efforts would contribute to the development of more reliable and efficient lightweight hybrid crashworthy structures for practical automotive safety applications.

Author's Declaration

Authors' contributions and responsibilities

M.S.F: Conceptualization, formal analysis, investigation, methodology, writing – original draft, writing – review & editing. K.A: Conceptualization, formal analysis, investigation, methodology. M.S.H: formal analysis, writing – review & editing. I.K.D.A: Investigation, methodology.

Funding

No funding information from the authors.

Availability of data and materials

All data are available from the authors.

Competing interests

The authors declare no competing interest.

Additional information

No additional information from the authors.

References

[1] X. Zhang, G. Cheng, Z. You, and H. Zhang, "Energy absorption of axially compressed thin-walled square tubes with patterns," *Thin-Walled Structures*, vol. 45, no. 9, pp. 737–746, Sep. 2007, doi: 10.1016/j.tws.2007.06.004.

[2] W. Abramowicz, "Thin-walled structures as impact energy absorbers," *Thin-Walled Structures*, vol. 41, no. 2–3, pp. 91–107, Feb. 2003, doi: 10.1016/S0263-8231(02)00082-4.

[3] J. Ma, S. Chai, and Y. Chen, "Geometric design, deformation mode, and energy absorption of patterned thin-walled structures," *Mechanics of Materials*, vol. 168, p. 104269, May 2022, doi: 10.1016/j.mechmat.2022.104269.

[4] F. Djamaluddin, S. Abdullah, A. K. Ariffin, and Z. M. Nopiah, "Optimization of foam-filled double circular tubes under axial and oblique impact loading conditions," *Thin-Walled Structures*, vol. 87, pp. 1–11, Feb. 2015, doi: 10.1016/j.tws.2014.10.015.

[5] W. Artha Wirawan, A. Zulkarnain, H. Boedi Wahjono, Jamaludin, and A. Tyas Damayanti, "The Effect of Material Exposure Variations on Energy Absorption Capability and pattern of Deformation Material of Crash Box of Three Segments," *Journal of Physics: Conference Series*, vol. 1273, no. 1, 2019, doi: 10.1088/1742-6596/1273/1/012081.

[6] M. Ceyhan and B. Yildiz, "Investigation of Crash Performance of Multi-Cell Crash-Boxes," *Çukurova Üniversitesi Mühendislik Fakültesi Dergisi*, vol. 38, no. 3, pp. 613–621, Oct. 2023, doi: 10.21605/cukurovaumfd.1377191.

[7] J. Zhang, S. Wang, C. Di, L. Zhang, H. Zhou, and L. Ning, "3G-optimization of multi-cell crash box cross-section of autobody based on crashworthiness," *Proceedings of the Institution of Mechanical Engineers, Part D: Journal of Automobile Engineering*, vol. 238, no. 5, pp. 887–899, Apr. 2024, doi: 10.1177/09544070221141506.

[8] X. Ma and X. Tian, "Crushing behaviour of a novel hybrid multi-cell structure," *Journal of the Brazilian Society of Mechanical Sciences and Engineering*, vol. 44, no. 9, p. 383, Sep. 2022, doi: 10.1007/s40430-022-03625-5.

[9] J. Xiong, Y. Zhang, L. Su, F. Zhang, and C. Wu, "Experimental and numerical study on mechanical behavior of hybrid multi-cell structures under multi-crushing loads," *Thin-Walled Structures*, vol. 170, p. 108588, Jan. 2022, doi: 10.1016/j.tws.2021.108588.

[10] A. Porwal, A. Tripathi, and P. Krishnasamy, "Frontal Crash Worthiness Performance of Bi-Tubular Corrugated Conical: Structures under Axial Loads at Low Velocity," 2020. doi: 10.4271/2020-01-0983.

[11] I. Choirotin, M. A. Choiron, A. Purnowidodo, and D. Bangun Darmadi, "Deformation Mode and Energy Absorption Analysis of Bi-Tubular Corrugated Crash Box Structure," *International Journal of Integrated Engineering*, vol. 13, no. 7, pp. 274–280, Nov. 2021, doi: 10.30880/ijie.2021.13.07.031.

[12] A. Saber, A. M. Amer, A. I. Shehata, H. A. El-Gamal, and A. Abd_Elsalam, "Recent Developments in Additively Manufactured Crash Boxes: Geometric Design Innovations, Material Behavior, and Manufacturing Techniques," *Applied Sciences*, vol. 15, no. 13, p. 7080, Jun. 2025, doi: 10.3390/app15137080.

[13] A. Mortazavi Moghaddam, A. Kheradpisheh, and M. Asgari, "A basic design for automotive crash boxes using an efficient corrugated conical tube," *Proceedings of the Institution of Mechanical Engineers, Part D: Journal of Automobile Engineering*, vol. 235, no. 7, pp. 1835–1848, Jun. 2021, doi: 10.1177/0954407021990921.

[14] F. G. Alabtah, E. Mahdi, and M. Khraisheh, "Energy absorption characteristics of a bio-inspired prepreg carbon fiber crash box under quasi-static axial compression," *Composites Part C: Open Access*, vol. 14, p. 100487, Jul. 2024, doi: 10.1016/j.jcomc.2024.100487.

[15] A. De Biasio, H. Ghasemnejad, S. Srimanosaowapak, and J. W. Watson, "Development of multi aluminium foam-filled crash box systems to improve crashworthiness performance of road Service vehicle," *European Journal of Mechanics - A/Solids*, vol. 109, p. 105433, Jan. 2025, doi: 10.1016/j.euromechsol.2024.105433.

[16] M. H. Mohd Hanid, S. Sharif, M. Ahmad, M. A. Suhaimi, C. Y. Khor, and K. A. Ismail, "Crashworthiness performance of thin-walled structures towards design configuration in vehicle crash boxes application: a review," *International Journal of Crashworthiness*, vol. 30, no. 6, pp. 704–734, Nov. 2025, doi: 10.1080/13588265.2025.2492975.

[17] S. K. Mert, M. Demiral, M. Altin, E. Acar, and M. A. Güler, "Experimental and numerical investigation on the crashworthiness optimization of thin-walled aluminum tubes considering damage criteria," *Journal of the Brazilian Society of Mechanical Sciences and Engineering*, vol. 43, no. 2, p. 113, Feb. 2021, doi: 10.1007/s40430-020-02793-6.

[18] K. Memane, A. Mashalkar, and P. Kumar, "A Review Thin-Wall-Tube Energy-Absorbing Structure : Crash-Box," *Journal of Physics: Conference Series*, vol. 2426, no. 1, p. 012060, Feb. 2023, doi: 10.1088/1742-6596/2426/1/012060.

[19] B. S. Kale, K. S. Bhole, N. A. Mandhare, and S. V Patil, "Finite element analysis and deployment of analytical hierarchical process for design of the structural framework for micro-actuators of vehicle crash box," *International Journal on Interactive Design and Manufacturing (IJIDeM)*, vol. 18, no. 10, pp. 6953–6963, Dec. 2024, doi: 10.1007/s12008-023-01219-6.

[20] H. Tan *et al.*, "Crashworthiness design and multi-objective optimization of a novel auxetic hierarchical honeycomb crash box," *Structural and Multidisciplinary Optimization*, vol. 64, no. 4, pp. 2009–2024, Oct. 2021, doi: 10.1007/s00158-021-02961-9.

[21] S. Wu, G. Zheng, G. Sun, Q. Liu, G. Li, and Q. Li, "On design of multi-cell thin-wall structures for crashworthiness," *International Journal of Impact Engineering*, vol. 88, pp. 102–117, Feb. 2016, doi: 10.1016/j.ijimpeng.2015.09.003.

[22] T. Chen, Y. Zhang, J. Lin, and Y. Lu, "Theoretical analysis and crashworthiness optimization of hybrid multi-cell structures," *Thin-Walled Structures*, vol. 142, pp. 116–131, Sep. 2019, doi: 10.1016/j.tws.2019.05.002.

[23] W. A. Wirawan *et al.*, "Crashworthiness characteristic of aluminum/composite hybrid tubes under axial compression," *Results in Engineering*, vol. 25, no. January, p. 103889, Mar. 2025, doi: 10.1016/j.rineng.2024.103889.

[24] R. Ardiansyah, F. K. Indriani, D. Hidayat, A. Tjahjono, A. Nurrohmad, and A. Marta, "Crashworthiness Performance Study of 3D-Printed Multi-Cell Tubes Hybridized with Aluminum Under Axial Quasi-Static Testing," *Automotive Experiences*, vol. 7, no. 3, pp. 567–578, Dec. 2024, doi: 10.31603/ae.12247.

[25] G. Zheng, T. Pang, G. Sun, S. Wu, and Q. Li, "Theoretical, numerical, and experimental study on laterally variable thickness (LVT) multi-cell tubes for crashworthiness," *International Journal of Mechanical Sciences*, vol. 118, pp. 283–297, Nov. 2016, doi: 10.1016/j.ijmecsci.2016.09.015.

[26] A. Vinod, J. Tengsuthiwat, R. Vijay, M. R.

Sanjay, and S. Siengchin, "Advancing additive manufacturing: <scp>3D</scp> -printing of hybrid natural fiber sandwich (<scp>Nona/Soy-PLA</scp>) composites through filament extrusion and its effect on thermomechanical properties," *Polymer Composites*, vol. 45, no. 9, pp. 7767–7789, Jun. 2024, doi: 10.1002/pc.28302.

[27] Z. U. Arif *et al.*, "Additive manufacturing of sustainable biomaterials for biomedical applications," *Asian Journal of Pharmaceutical Sciences*, vol. 18, no. 3, p. 100812, May 2023, doi: 10.1016/j.ajps.2023.100812.

[28] Z. G. Mohammadsalih, M. Muaw-widzah, V. U. Siddiqui, and S. M. Sapuan, "Mechanical properties of wood fibre filled polylactic acid (PLA) composites using additive manufacturing techniques," *Journal of Natural Fibers and Polymer Composites*, vol. 2, no. 2, p. 3, 2023.

[29] W. A. Wirawan *et al.*, "Collapse Behavior and Energy Absorption Characteristics of Design Multi-Cell Thin Wall Structure 3D-Printed Under Quasi Statistic Loads," *Automotive Experiences*, vol. 7, no. 1, pp. 149–160, May 2024, doi: 10.31603/ae.10892.

[30] G. Sun, D. Chen, G. Zhu, and Q. Li, "Lightweight hybrid materials and structures for energy absorption: A state-of-the-art review and outlook," *Thin-Walled Structures*, vol. 172, p. 108760, Mar. 2022, doi: 10.1016/j.tws.2021.108760.

[31] X. Fu, X. Zhang, and Z. Huang, "Axial crushing of Nylon and Al/Nylon hybrid tubes by FDM 3D printing," *Composite Structures*, vol. 256, p. 113055, Jan. 2021, doi: 10.1016/j.compstruct.2020.113055.

[32] D. Hidayat *et al.*, "Experimental investigation on axial quasi-static crushing of Al/PLA hybrid tubes," *Journal of Physics: Conference Series*, vol. 2551, no. 1, p. 012008, Jul. 2023, doi: 10.1088/1742-6596/2551/1/012008.

[33] E. Kösedağ and D. İşler, "Effect of section geometry and material type on energy absorption capabilities of crash boxes," *Karaelmas Fen ve Mühendislik Dergisi*, vol. 13, no. 1, pp. 42–51, 2023, doi: 10.7212/karaelmasfen.1150591.

[34] G. Jiga, Ş. Stamin, G. Dinu, D. Vlăsceanu, and D. Popovici, "Material and shape crash-box influence on the evaluation of the impact energy absorption capacity during a vehicle collision," *Ciência & Tecnologia dos Materiais*, vol. 28, no. 1, pp. 67–72, Jan. 2016, doi: 10.1016/j.ctmat.2016.03.001.

[35] S. Wesselmecking, M. Kreins, M. Dahmen, and W. Bleck, "Material oriented crash-box design-Combining structural and material design to improve specific energy absorption," *Materials & Design*, vol. 213, p. 110357, 2022, doi: 10.1016/j.matdes.2021.110357.

[36] H. Liang, C. Lu, Y. Pu, B. Liu, and D. Wang, "Data-driven initial peak crushing force prediction of hybrid tubes," *International Journal of Mechanical Sciences*, vol. 271, p. 109141, Jun. 2024, doi: 10.1016/j.ijmecsci.2024.109141.

[37] J. Dong, Y. Wang, F. Jin, and H. Fan, "Crushing behaviors of buckling-induced metallic meta-lattice structures," *Defence Technology*, vol. 18, no. 8, pp. 1301–1310, Aug. 2022, doi: 10.1016/j.dt.2021.07.014.

[38] H. Nikkhah, A. Baroutaji, Z. Kazancı, and A. Arjunan, "Evaluation of crushing and energy absorption characteristics of bio-inspired nested structures," *Thin-Walled Structures*, vol. 148, p. 106615, Mar. 2020, doi: 10.1016/j.tws.2020.106615.

[39] A. Tasdemirci *et al.*, "Crushing behavior and energy absorption performance of a bio-inspired metallic structure: Experimental and numerical study," *Thin-Walled Structures*, vol. 131, pp. 547–555, Oct. 2018, doi: 10.1016/j.tws.2018.07.051.

[40] Z. Fan, G. Lu, and K. Liu, "Quasi-static axial compression of thin-walled tubes with different cross-sectional shapes," *Engineering Structures*, vol. 55, pp. 80–89, Oct. 2013, doi: 10.1016/j.engstruct.2011.09.020.

[41] S. K. Tak and M. A. Iqbal, "Axial compression behaviour of thin-walled metallic tubes under quasi-static and dynamic loading," *Thin-Walled Structures*, vol. 159, p. 107261, Feb. 2021, doi: 10.1016/j.tws.2020.107261.

[42] W. Liu, J. Lian, S. Münstermann, C. Zeng, and X. Fang, "Prediction of crack formation in the progressive folding of square tubes during dynamic axial crushing," *International Journal of Mechanical Sciences*, vol. 176, p. 105534, Jun.

2020, doi: 10.1016/j.ijmecsci.2020.105534.

[43] W. Chen and T. Wierzbicki, "Relative merits of single-cell, multi-cell and foam-filled thin-walled structures in energy absorption," *Thin-Walled Structures*, vol. 39, no. 4, pp. 287–306, Apr. 2001, doi: 10.1016/S0263-8231(01)00006-4.

[44] X. Li *et al.*, "Influence of dynamic compressive loading on the in vitro degradation behavior of pure PLA and Mg/PLA composite," *Acta Biomaterialia*, vol. 64, pp. 269–278, Dec. 2017, doi: 10.1016/j.actbio.2017.08.004.

[45] L. Tripathi, O. Singh, and B. K. Behera, "3-D woven honeycomb structures and their composites," *Textile Progress*, vol. 56, no. 2, pp. 231–322, Apr. 2024, doi: 10.1080/00405167.2024.2318182.

[46] H. Liang, Y. Zhao, S. Chen, F. Ma, and D. Wang, "Review of Crashworthiness Studies on Cellular Structures," *Automotive Innovation*, vol. 6, no. 3, pp. 379–403, Aug. 2023, doi: 10.1007/s42154-023-00237-0.

[47] N. N. Hussain, S. P. Regalla, Y. V. D. Rao, T. Dirgantara, L. Gunawan, and A. Jusuf, "Drop-weight impact testing for the study of energy absorption in automobile crash boxes made of composite material," *Proceedings of the Institution of Mechanical Engineers, Part L: Journal of Materials: Design and Applications*, vol. 235, no. 1, pp. 114–130, Jan. 2021, doi: 10.1177/1464420720952813.

[48] S. Boria, J. Obradovic, and G. Belingardi, "Experimental and numerical investigations of the impact behaviour of composite frontal crash structures," *Composites Part B: Engineering*, vol. 79, pp. 20–27, Sep. 2015, doi: 10.1016/j.compositesb.2015.04.016.

[49] S. Heimbs, P. Middendorf, S. Kilchert, A. F. Johnson, and M. Maier, "Experimental and Numerical Analysis of Composite Folded Sandwich Core Structures Under Compression," *Applied Composite Materials*, vol. 14, no. 5–6, pp. 363–377, Nov. 2007, doi: 10.1007/s10443-008-9051-9.

[50] A. Baroutaji, A. Arjunan, G. Singh, and J. Robinson, "Crushing and energy absorption properties of additively manufactured concave thin-walled tubes," *Results in Engineering*, vol. 14, p. 100424, Jun. 2022, doi: 10.1016/j.rineng.2022.100424.

[51] A. Baroutaji, A. Arjunan, M. Stanford, J. Robinson, and A. G. Olabi, "Deformation and energy absorption of additively manufactured functionally graded thickness thin-walled circular tubes under lateral crushing," *Engineering Structures*, vol. 226, p. 111324, Jan. 2021, doi: 10.1016/j.engstruct.2020.111324.